Experience-dependent modulation of behavioral features in sensory navigation of nematodes and bats revealed by machine learning

Short Title: Machine learning extraction of behavioral features

Authors: Shuhei J. Yamazaki[1], Yosuke Ikejiri[1], Fumie Hiramatsu[1], Kosuke Fujita[1, 5], Yuki Tanimoto[1, 6], Yasufumi Yamada[2], Koichi Hashimoto[3], Shizuko Hiryu[2], Takuya Maekawa[4], Koutarou D. Kimura[1*]

Affiliations

[1]Department of Biological Sciences, Graduate School of Science, Osaka University, Toyonaka, Osaka 560-0043, Japan

[2]Faculty of Life and Medical Sciences, Doshisha University, Kyotanabe, Kyoto 6100321, Japan

[3]Graduate School of Information Sciences, Tohoku University, Sendai, Miyagi 980-8579, Japan

[4]Department of Multimedia Engineering, Graduate School of Information Science and Technology, Osaka University, Suita, Osaka 565-0871, Japan

[5]Present address: Department of Ophthalmology, Graduate School of Medicine, Tohoku University, Sendai, Miyagi 980-8574, Japan

[6]Present address: RIKEN Brain Science Institute, Wako, Saitama 351-0198, Japan

*Correspondence: kokimura-lab@umin.ac.jp or kokimura@bio.sci.osaka-u.ac.jp

Classification: Biological Sciences, Neuroscience

ABSTRACT

Animal behavior is the integrated output of multiple brain functions. However, understanding how multiple brain functions affect behavior has been difficult. In order to decipher dynamic brain functions from time-series of behavioral data, we developed a machine learning strategy that extracts distinguishing behavioral features of sensory navigation. We first investigated experience-dependent enhancement of odor avoidance behavior of the nematode *Caenorhabditis elegans*. We segmented worms' trajectories during olfactory navigation into two behavioral states, analyzed 92 features of the states, and automatically extracted 9 distinguishing features modulated by prior odor experience using a statistical index, the gain ratio. The extracted features included ones previously unidentified, one of which indicated that the prior odor experience lowers worms' behavioral responses to a small increase in odor concentration, causing enhanced odor avoidance. Consistently, calcium imaging analysis under gradually increased odor stimulation revealed that the response of ASH nociceptive neurons to a small odor increase was significantly reduced after prior odor experience. In addition, based on extracted features, multiple mutant strains were categorized into several groups that are related to physiological functions of the mutated genes, suggesting a possible estimation of unknown gene function by behavioral features. Furthermore, we also extracted behavioral features modulated by experience in acoustic navigation of bats. Thus, our results demonstrate that, regardless of animal species, sensory modality, and spatio-temporal scale, behavioral features during navigation can be extracted by machine learning analysis, which may lead to the understanding of information processing in the brain.

Keywords: Navigation, Machine Learning, Behavior

INTRODUCTION

Brain activity can be measured as time series vector data of a large number of neural activities using simultaneous optical monitoring recently (1, 2). Behavior, the integrated output of multiple brain functions such as sensory perception, memory, emotion, and decision-making, however, is still analyzed in classic ways and insufficiently studied using simple and subjectively chosen measures, such as velocity, migratory distance, and/or the probability of reaching to a particular goal. This large asymmetry in data between neural activity and behavior has emerged as one of the significant issues in modern neuroscience (3-5). One cause for this problem is the difficulty in the analysis of behavior: Although machine-vision techniques over small areas and GPS-based tracking over large areas allow us to continuously monitor the positions and/or postures of animals, it is still unclear which aspects of behavioral features, such as speed, direction, their duration and rate of change, are related to an animal's dynamic brain activity.

One way to solve this problem is to use machine learning. Machine learning is a method of extracting latent patterns and discovering knowledge from a large amount of data (6). Machine learning-based behavioral analyses of model invertebrates, such as the fruit fly *Drosophila melanogaster* and the nematode *Caenorhabditis elegans*, have been performed because these model animals are suitable for machine vision monitoring of their behavior due to their small size and relatively simple behavioral patterns (7-13). Furthermore, these animals have relatively small neural circuits, and multiple genetic techniques are available, suggesting that comprehensive analysis of brain function at

behavioral, neuronal, and molecular levels is feasible. These analyses have provided new insights into behavioral states and behavioral motifs during voluntary movement, as well as the relationships between optogenetic activation of neurons and behavioral responses. However, machine learning has not been used to understand the brain activity related to sensory behaviors: How is environmental information transformed into behavioral responses through sensory perception and decision-making, as well as its modulation by memory and/or emotion? The lack of research in this topic is likely due to the fact that these invertebrate model animals are too small to accurately and easily measure sensory input during behavior. In addition, even when sensory input can be measured, the method to effectively reveal the dynamic relationships between sensory input and behavioral output has not been established.

In the present study, we aimed to establish a method to objectively and comprehensively analyze behavioral features that possibly link sensory input and behavioral output. For that purpose, we analyzed two types of sensory navigation that have been monitored quantitatively but are different in modality and spatio-temporal scale—olfactory navigation of *C. elegans* and acoustic navigation of the bat *Rhinolophus ferrumequinum nippon*—using machine learning. In particular, we focused on experience-dependent modulation (i.e., "learning"; to avoid confusion with machine learning analysis, we do not use this term for biological learning hereafter) of navigation as a model for efficient extraction of differences in behavioral features. In *C. elegans*, experience-dependent behavioral modulation has been studied in thermotaxis and salt-taxis, in which worms move in a preferred direction by changing the frequency

96 of directional changes depending on the intensity of the sensory stimulus (14).
97 Consistently, changes in neural activity to a stepwise stimulus change have been
98 revealed by calcium imaging mostly of immobilized worms and in a few cases of freely
99 moving worms (15-20). However, it has not been fully clarified how those behaviors
100 are regulated by neural activity that responds to slight changes in stimuli during
101 navigation in a sensory gradient as well as how the behavioral and neural responses are
102 modulated by experience. Furthermore, although large scale analyses of mutant strains
103 are available (12, 21), methods for effectively analyzing the differences in
104 experience-dependent modulation of sensory behaviors of mutant strains have not been
105 established.
106
107 To reveal experience-dependent modulations of olfactory navigation in worms, we
108 extracted prominent features of behavior and their relationships to odor stimuli using
109 machine learning. For this, we segmented the animals' navigation into two behavioral
110 states and, for individual states, calculated the gain ratio, a statistical index used in
111 decision tree analysis to identify features that distinguish the data in different classes
112 (22). In the present study, we analyzed 92 features of behavior and sensory information
113 from each of ~200 behavioral states of wild-type worms either with or without a prior
114 odor experience (25 worms per condition) and found that 9 features are modulated in an
115 experience-dependent manner. One of the extracted features, the reduction in behavioral
116 response to a small increase in odor concentration, was consistent with a change in
117 neuronal activity revealed by calcium imaging. In addition, we calculated gain ratios to
118 identify the experience-dependent changes in olfactory navigation of multiple mutant

119 strains and found that the mutants were categorized into several groups based on
120 behavioral features, which reflect physiological functions of the mutated genes.
121 Furthermore, we also identified experience-dependent modulation of behavioral
122 features from bat acoustic navigation. Thus, we propose that machine learning analysis
123 with gain ratios is an efficient strategy to reveal features of animal behavior in general.
124

125 **METHODS**

126 **Cultivation of worms**

127 The techniques used for culturing and handling *C. elegans* strains have been essentially
128 described previously (23). Wild type Bristol strain RRID:WB-STRAIN:N2_Male and
129 mutant strains RRID:WB-STRAIN:MT1219 *egl-3(n589)*, RRID:WB-STRAIN:VC671
130 *egl-3(ok979)*, RRID:WB-STRAIN:CX4544 *ocr-2(ak47),* RRID:WB-STRAIN:JC1636
131 *osm-9(ky10)*, RRID:WB-STRAIN:JC0570 *tax-4(p678)* were obtained from the
132 Caenorhabditis Genetics Center (University of Minnesota, USA).
133 RRID:WB-STRAIN:KDK1 dop-3*(tm1356)* was originally obtained from National
134 BioResource Project (Japan) and backcrossed five times with N2 .
135

136 **Analysis of worms' olfactory navigation**

137 A 2-nonanone avoidance assay was performed as described previously (24, 25). Briefly,
138 2-3 young adult hermaphrodite worms grown synchronously were placed in the center
139 of a 9-cm nematode growth media (NGM) plate, and 2 μL of 30% 2-nonanone (cat. no.
140 132-04173; Wako, Japan) diluted in EtOH (cat. no. 0057-00456; Wako, Japan) were
141 dropped in two spots on the surface of the NGM plate (Fig. 1A top), and the worms'

142 behavior was recorded for 12 min. This assay was performed under the following three
143 conditions: the worms cultivated on NGM plates with their food bacteria
144 RRID:WB-STRAIN:OP-50 were briefly washed with NGM buffer and subjected to the
145 assay ("naive" condition), or they were subjected to the assay after 1 h of preexposure to
146 0.6 μL of 15% 2-nonanone diluted in EtOH or to only EtOH spotted on the lid of a
147 NGM plate without food ("preexp" and "mock" conditions, respectively). We added the
148 mock-treated control to confirm that 1-h starvation did not affect the odor avoidance
149 behavior of worms and to extract behavioral features modulated by the odor
150 preexposure compared to the naive and the mock-treated controls. Images of worms the
151 NGM plate during odor avoidance assay were acquired by a high-resolution USB
152 camera (DMK 72AUC02; The Imaging Source, USA) with a lens (LM16JC5MW;
153 Kowa, Japan) at 1 Hz for 12 min. From the recorded images, the coordinates of
154 individual animals' centroids were acquired using Move-tr/2D software (Library Co.,
155 Ltd., Tokyo, Japan) and used for the following analysis.
156
157 Similar to worms' other sensory behaviors, trajectories in the 2-nonanone avoidance
158 assay can be divided into two states: "run", a relatively long period of straight
159 movement, and "pirouette", a period of short movements interrupted by frequent
160 reversals and turns (24, 26). Angular change per s was calculated from the centroid
161 coordinates, and movements of 1 s with angular change larger than 90° were classified
162 as a turn. A histogram of turn intervals was fitted by two exponentials, suggesting that
163 turn intervals are regulated by two probabilistic mechanisms (25, 26). The time of the
164 intersection of the two exponentials was defined as t_{crit}, and turn intervals longer or

shorter than the t_{crit} were classified as runs or included in pirouettes, respectively. t_{crit} was calculated for the control (i.e., naive plus mock-treated) condition for wild-type and mutant strains, respectively. In this study, we analyzed features of runs but not of pirouettes except for their duration because pirouettes appear to have little effect on odor avoidance (25). Excel 2010 (Microsoft Corp.) was used for these calculations. The odor concentrations that worms experienced at specific spatio-temporal points were calculated according to the dynamic odor gradient model based on the measured odor concentration (19).

Bats

As previously described, three adult Japanese horseshoe bats (*Rhinolophus ferrumequinum nippon*, body length: 6.0–8.0 cm, body mass: 20–30 g) were captured from natural caves in Hyogo and Osaka prefectures in Japan (27). The bats were housed in a temperature- and humidity-controlled colony room [4 (L) × 3 (W) × 2 m (H)] with a 12-h-on/12-h-off light cycle at Doshisha University in Kyoto, Japan. The bats were allowed to fly freely and given access to mealworms and water. Captures were conducted under license and in compliance with current Japanese law. All experiments complied with the Principles of Animal Care, publication no. 86-23, revised 1985, of the National Institutes of Health, and with current Japanese law. All experiments were approved by the Animal Experiment Committee of Doshisha University.

Bat acoustic navigation

Methods for acoustic navigation measurement in bats have been described elsewhere

188 (Yamada et al., in revision). In brief, the experiments were conducted in a flight
189 chamber, which was constructed of steel plates [9 (L) × 4.5 (W) × 2.5 m (H)] under
190 lighting with red filters (>650 nm) to avoid visual effects on the bats. An obstacle
191 environment was constructed using plastic chains (4 cm in diameter) that were
192 suspended from the ceiling of the chamber. The chains were arranged at 15-cm intervals
193 in the *x*-axis and at 22-cm intervals in the *y*-axis so that the bat was forced to fly in an
194 S-shaped pattern without passing between chains. With this layout, three naive bats
195 were used: each bat was observed for 12 continuous repeated flights so that
196 echolocation behaviors in unfamiliar and familiar spaces could be compared. In this
197 study, the initial three flights were defined as unfamiliar flights, and the last three flights
198 were defined as familiar flights.
199
200 The flight behavior of the bats was recorded using two digital high-speed video cameras
201 (MotionPro X3; IDT Japan, Inc., Japan) at 125 frames/s, which were located in the left
202 and right corners of the flight chamber. Based on a direct linear transformation
203 technique, the successive 3D positions of the flying bats, as well as the locations of
204 other objects, were reconstructed using motion analysis software (DIPPMotionPro
205 ver. 2.2.1.0; Ditect Corp., Japan). The flight velocity vector of the bat was calculated as
206 the time derivative of the coordinates of its flight trajectory.
207
208 **Behavioral parameters included in a feature vector**
209 For the machine learning analysis of worm olfactory navigation, the following
210 behavioral features were calculated for each run from the centroid coordinates of the

worms: start time (*RunTime*), serial number (*RunNum*), velocity (*V*), bearing (*B*), odor concentration that a worm experienced during run (*C*), directionality ratio (*Dir*) (28), run's curvature (called weathervane; *WV*) (29), run duration (*RunDur*), and duration of pirouette just before the run (*PirDur*). Time-differential values were calculated for *V* (*dV*), *B* (*dV*), and *C* (*dC*). For these values, the average (*Ave*) during a run as well as average values over 2 s at the initiation (*Ini*) and at the termination (*Ter*) of a run were also calculated. For *Ini* and *Ter*, 0-2 s after the initiation and 2-4 s before the termination of a run were used; we did not use 0-2 seconds before the termination because previous studies revealed that a worm's speed drops largely during this period (25, 26). Although the time windows for worms were set based on the previous studies, the optimal time windows for bats were calculated by machine learning (see below). In addition, to analyze whether these features are independent for each run (in other words, whether any long-term trend among runs across a pirouette exists), we also calculated hysteretic effects (Δ) of these run features between successive runs for *V*, *dV*, *B*, *dB*, *C*, and *dC*—in fact, a certain relationship between bearings before and after a pirouette (*B_Ini*Δ*Ter*) has been reported in salt-taxis (26). For this, *Ave*, *Ini,* or *Ter* of each run feature was subtracted from any of the previous run features. Hysteretic effects were calculated for just one feature for *RunDur*, *PirDur*, and *WV*, which only possess one value per run, and not calculated for *RunTime* and *RunNum*. A total of 92 features were calculated by combining all these features.

For analysis of changes in the flight of the bats, the following behavioral features in each flight were calculated from the coordinates of the animals and obstacles:

234 three-dimensional flight velocity (*V*), horizontal and vertical bearings of the flight
235 (*B_hori* and *B_vert*, respectively), distance (*R_obs*) and bearing (*B_obs*) of the bat to
236 the nearest edge point of the obstacle chain array, longitudinal directional distance to
237 the frontal chain array (*R_x*), lateral directional distance to the inside pitch of the chain
238 array (*R_y*). Time-differential values were calculated for *V* (*dV*), *B* (*dB*), *dB* (*ddB*), and
239 the flight height (*dH*), which were calculated with frame units of the high-speed video
240 cameras (1/125 s). All flight trajectories were divided into three segments: earlier,
241 middle, and later terms. The time window for the analysis of each behavioral feature
242 was 0.1, 0.2, or 0.3 s before or when ($t = 0$) passing through the chain array. A total of
243 42 features were calculated by combining all these features.
244
245 Excel 2010 and Visual C# (Microsoft) were used for the calculations, and the
246 Beeswarm package for R software (The R Project) was used for the scattered plot of
247 data. These parameters are listed in Table 1 for worms and in Table 4 for bats.
248
249 **Behavioral classification with gain ratio**
250 In order to extract useful features, we calculated the gain ratio used in C4.5 decision tree
251 analysis (30) for each feature. In decision tree analysis, the amount of information,
252 which is acquired when a group of data is divided into sub-groups by a certain feature,
253 is calculated as information gain. In other words, when dividing a group into sub-groups
254 by applying a certain feature, information gain is an index indicating the amount of the
255 increased bias of data in the sub-groups after the division. The information gain was
256 then divided by split info, a degree of division, for normalization to compute the gain

257 ratio. For worm olfactory navigation, we extracted behavioral features that have
258 positive gain ratios in naive versus preexposed worms or in mock-treated versus
259 preexposed worms. Then, we chose the features that were common in both comparisons
260 as "features modulated in experience-dependent manner". For bat acoustic navigation,
261 behavioral features were extracted from the comparison of unfamiliar flights (1st-3rd)
262 and familiar (10th-12th) flights. Weka software (the University of Waikato, New
263 Zealand) (31) was used for the calculation.
264
265 **Calcium imaging**
266 Calcium imaging of the worms' ASH neurons was performed according to a previous
267 report (19). Briefly, transgenic strains expressing GCaMP3 (32) and mCherry (33) in
268 ASH sensory neurons under the *sra-6* promoter (KDK70034 and KDK70072; 20 ng/µl
269 of *sra-6p::GCaMP3*, 20 ng/µl of *sra-6p::mCherry*, 10 ng/µl of *lin-44p::GFP*, 50 ng/µl
270 of PvuII-cut N2 genomic DNA as a carrier in N2 background) were placed on an NGM
271 agar plate on a robotic microscope system, OSB2 (19). Although these transgenic
272 worms were immobilized with the acetyl choline receptor agonist levamisole (34) for
273 high-throughput data acquisition by simultaneous imaging of multiple worms, the
274 previous study revealed that the ASH activity is essentially unaffected by
275 levamisole-treatment (19). For these worms, a constant gas flow of 8 mL/min was
276 delivered, in which the mixture rate of 2-nonanone gas versus the air was changed to
277 make a temporal gradient of the odor concentration. The temporal change in odor
278 concentration was measured by a custom-made semiconductor sensor before and after
279 the series of calcium imagings on each day. The fluorescence signals of GCaMP3 and

280 mCherry in ASH neurons were divided into two channels using W-View (Hamamatsu,
281 Japan), an image splitting optic, and captured by an EM-CCD camera (ImagEM;
282 Hamamatsu, Japan) at 1 Hz. The intensities of fluorescence signals from cell bodies
283 were extracted and quantified by ImageJ (NIH) after background subtraction. The
284 average ratio over 30 s prior to the odor increase was used as a baseline (F_0), and the
285 difference from F_0 (ΔF) was used to calculate the fluorescence intensities of GCaMP3
286 and mCherry ($F = \Delta F/F_0$). The ratio between florescence intensities of GCaMP and
287 mCherry (GCaMP/mCherry) was used in the figure.
288
289 **Statistical analysis**
290 For comparisons of behavioral features among naive, mock-treated, and preexposed
291 worms, the Kruskal-Wallis multiple comparison test followed by the *post hoc* Dunn's
292 test were used (Fig. 2, 3 and 4), except for in the analysis of directional data, for which
293 the Mardia-Watson-Wheeler test was used. The calculations were performed with Prism
294 ver. 5.0 for Mac OSX (GraphPad Software, CA, USA), R (The R Project) or SPSS
295 version 23 (IBM Corp.).
296
297 **RESULTS**
298 **A strategy for extracting features of sensory navigation that were modulated by**
299 **prior experience**
300 In this study, we aimed to extract behavioral features using machine learning to
301 understand changes in information processing in the brain during sensory navigation.
302 However, identifying characteristic changes in behavior and sensory stimulus during

303 navigation has been difficult. It is because sensory stimulus in general changes
304 gradually and continuously during navigation, which may cause gradual or sudden
305 response at some aspects of behavior with certain probabilities. In order to efficiently
306 extract behavioral features of sensory navigation by machine learning, we considered
307 the following points for the analysis: (1) segmenting behavioral states, (2) representing
308 the animal's position as a single point, (3) calculating sensory information, and (4) using
309 a statistical index, gain ratio.
310
311 ***Segmenting behavioral states***
312 Segmentation is one of the important preprocessing steps of a large dataset for effective
313 analysis (35).We considered an animal's navigation to be a series of transitions among a
314 limited number of behavioral states for a certain period, and we analyzed features in
315 each of the behavioral states instead of analyzing features in an entire navigation
316 trajectory or in very short temporal unit (i.e., second or sub-second). For worm
317 olfactory navigation, we segmented the navigation into two well-established behavioral
318 states: runs and pirouettes (14, 26; see METHODS for details). For bat acoustic
319 navigation, we considered the period from passing one obstacle (or from the starting
320 point) until passing the next obstacle as one behavioral state.
321
322 ***Representing animal's position as a point***
323 During a behavioral state in navigation, animals move a certain distance. For the sake of
324 proper dimensionality reduction, we calculated the trajectories of a point representing
325 animal's position (centroid for worms and head position for bats), instead of the posture

326 of an animal, whose description requires more detailed spatial and temporal
327 information.
328
329 ***Sensory information***
330 Sensory information is a key factor affecting an animal's behavior. However, because
331 of technical difficulties, it has been included in the analysis of sensory navigation only
332 in a few cases for small model animals (17, 19, 36). We included the information of
333 odor concentration, which changes dynamically during navigation of worms, as
334 revealed by the direct measurement of odor concentrations in specific spatio-temporal
335 points in a behavioral arena (19).
336
337 ***Gain ratio***
338 To comprehensively examine behavioral features that can be modulated by prior
339 experience, we focused on a statistical index used in machine learning-based
340 classification analysis. In general, classification analysis is the task of classifying new,
341 unlabeled data into appropriate classes using characteristic features and their parameters
342 that have been extracted from the known class-labeled data. In the present study,
343 however, the classification itself was not meaningful because the data were already
344 classified, such as with or without prior experience or wild-type versus mutant strains.
345 Instead, we focused on the procedure in the classification that finds features useful for
346 distinguishing between the two classes. In other words, behavioral features modulated
347 by prior experience should be able to effectively classify the behavioral data of animals
348 with or without this experience.

349

350 For this purpose, we chose to use gain ratio, the index for decision tree analysis (22).
351 Binary decision tree analysis is performed to split a data set into two sub-groups by
352 automatically selecting the best feature and its parameter that has the largest
353 information gain, the difference of the uncertainty ("information entropy") before and
354 after division; each data point is classified into either of the sub-classes based on
355 whether it has a larger or smaller value than the threshold. When applied for binary
356 classification, decision tree analysis automatically evaluates the classification
357 performance of all of a large number of features that are designed by the researchers.
358 The result of this analysis is the extraction of certain features, which allows us to easily
359 understand the usefulness of particular features for the classification. This is a
360 substantial difference from the analysis by support vector machines and/or deep neural
361 networks, where the relationships between features of the data and the classification are
362 not easily discernible (see DISCUSSION).
363

364 **Behavioral features modulated by the prior experience in worm odor avoidance**
365 **behavior**

366 We analyzed the experience-dependent enhancement of odor-avoidance behavior of *C.*
367 *elegans* as a model. We have reported that preexposure of worms to the repulsive odor
368 2-nonanone causes enhancement of avoidance behavior to the odor. After 1 h of
369 preexposure, worms migrate farther away from the odor source as a type of
370 non-associative middle-term learning (24). A series of genetic analyses indicated that
371 neuropeptide and dopamine signaling pathways are required for acquisition and

372 execution of the odor memory, respectively (25), suggesting that this non-associative
373 middle-term memory is caused by a circuit-level modulation of neural activity rather
374 than simple sensory sensitization.
375
376 Previous studies analyzed several features and revealed that run duration is the major
377 behavioral change caused by odor preexposure, likely because of reduction in the
378 pirouette initiation rate (24, 25). However, this did not rule out the possibility that other
379 behavioral features play more profound effects. Moreover, multiple mutant strains
380 exhibit their own abnormalities in the enhanced odor avoidance behavior (see below),
381 although identification of the features modulated in each mutant strain is
382 time-consuming and laborious. To reveal features modulated by prior experience
383 comprehensively and effectively, we calculated the gain ratio by comparing naive
384 versus preexposed and mock-treated versus preexposed animals, and we considered
385 features that were extracted from both comparisons.
386
387 In the machine learning analysis, we calculated gain ratios of 92 features (Fig. 1 and
388 Table 1; see METHODS for details) and extracted 18 and 15 features from the
389 comparisons of naive versus preexposed and mock-treated versus preexposed worms,
390 respectively (Table 2). Nine features were shared between the two comparisons,
391 suggesting that those features were modulated by the prior experience to cause the
392 enhanced odor avoidance (Table 2 and Fig. 2A). These features are related to run
393 duration (*RunDur*), temporal differences in bearing (*dB_X*), odor concentration (*C_X*),
394 and its temporal difference during runs (*dC_X*). Modulation of run duration (*RunDur*;

395 Fig. 2B) by the prior odor experience was previously revealed by traditional analysis
396 (24). Thus, this result demonstrates the validity of the machine learning analysis.
397
398 Experience-dependent modulations of temporal differences in bearing (*dB_X*; Fig. 2C
399 for example and Table 2) have not been revealed previously. Its contribution to the
400 enhancement of avoidance distance, however, are unclear. Differences between the
401 average or the terminal bearing change and the previous initial value (*dB_Ave*Δ*Ini* or
402 *dB_Ter*Δ*Ini*) were also extracted (Table 2), while the differences were likely due to the
403 modulation in the previous initial value (Δ*Ini*), not due to the change in hysteretic
404 effects.
405
406 Odor stimuli during runs, which likely drive the worms' odor avoidance behavior, were
407 also found to be modulated in several aspects: the initial, terminal, and average odor
408 concentration (*C_Ini*, *C_Ter*, and *C_Ave*), and the terminal and average odor
409 concentration change (*dC_Te*r and *dC_Ave*) (Table 2; Fig. 2D and E for *C_Ave* and
410 *dC_Ave*, respectively, for examples). However, this result does not directly imply that
411 the lower odor concentration is the causal reason for the enhanced avoidance distance;
412 one possible scenario is that, because the odor-experienced worms were located farther
413 away from the odor source, they sensed a lower concentration of the odor.
414
415 Because the terminal and average values of odor concentration change (*dC_Te*r and
416 *dC_Ave*) were extracted, and because a previous study demonstrated that worm odor
417 avoidance behavior depends on *dC*, rather than *C*, at least in naive conditions (19), we

418 investigated these features more in detail. We compared ensemble averages of *dC/dt*
419 that worms sensed during the last 30 s of each run (Fig. 2F). Interestingly, although
420 most of the control (*i.e.* naive and mock-treated) worms sensed 2-3 μM odor
421 concentrations (Fig. 2D), *dC/dt* at the end of each run was ± 0.1 nM/s on average (Fig.
422 2F; 0.09 ± 0.72 and -0.09 ± 0.76 nM/s for naive and mock-treated animals, respectively).
423 This result suggests that, to initiate a pirouette, worms respond to a subtle odor
424 concentration change, of which the magnitude is 1/20,000 - 1/30,000 of the odor
425 concentration itself per second. Even considering that sensory information is temporally
426 integrated for a few seconds during worm chemosensory navigation (19, 37), this value
427 is far lower than the general psychological threshold for sensory signals: The lower
428 threshold of signal change (ΔS) is more than 1/100 of the signal intensity (S) (38).
429
430 This extreme sensitivity to positive *dC/dt* was modulated by prior experience of the
431 odor. The terminal *dC/dt* was significantly higher than in naive and mock-treated
432 animals (1.58 ± 0.6 nM/s compared to the values in the previous paragraph; $p < 0.01$,
433 the Kruskal-Wallis multiple comparison test followed by the *post hoc* Dunn's test). This
434 change in terminal *dC/dt* could be the cause for the enhanced odor avoidance behavior
435 and suggest the following model: the worms without prior experience of the odor are
436 highly sensitive to a slight increase in odor concentration during a run, which is a sign
437 of inappropriate movement toward the source of the repulsive odor, and they respond to
438 it by initiating a pirouette. In contrast, the worms with prior odor experience ignore the
439 slight odor increase and continue the run, which leads to a longer run duration (Fig.
440 2G).

441

442 **The responsiveness of sensory neurons to odor increases was modulated by odor**

443 **experience**

444 If the change in sensitivity to positive *dC/dt* is the causal reason for the enhanced odor

445 avoidance behavior, it should be associated with changes in neural activity. Thus, we

446 analyzed the responsiveness of a likely candidate group of neurons, ASH nociceptive

447 neurons (39, 40). Previously we established the OSB2 microscope system that allows

448 for calcium imaging of *C. elegans* neurons *in vivo* under odor stimuli resembling ones

449 that worms experience during the odor avoidance assay in the plates (19). Using the

450 OSB2 system, we found that ASH neurons are the major sensory neurons to cause

451 pirouettes upon increases in 2-nonanone concentration (19). However, whether the ASH

452 response is modulated by 2-nonanone experience has not been studied.

453

454 We found that ASH responses were modulated by prior odor experience in a manner

455 consistent with the behavioral modulation. When the worms were stimulated with 5

456 nM/s odor increase, which is the lowest rate of change to cause the threshold-level

457 behavioral response in the previous study (19), ASH neurons in naive as well as

458 mock-treated worms exhibited robust responses (Fig. 3A and B). However, the ASH

459 responses were significantly reduced in the preexposed animals (Fig. 3B and C). This

460 result suggests that prior odor experience causes the reduced response to the odor

461 increase, which causes longer run durations and enhanced odor avoidance behavior.

462

463 **Extracted behavioral features of mutant strains correspond to gene functions**

464 We also investigated whether feature extraction from behavior of mutant strains can
465 allow us to understand relationships between chemosensory behavior and gene
466 functions in the nervous system. By calculating gain ratios, we analyzed mutants of
467 genes that are known to be involved in the experience-dependent modulation of
468 2-nonanone avoidance behavior, such as that for proprotein convertase (required for
469 neuropeptide signaling), EGL-3 (41), and the D2-type dopamine receptor DOP-3 (25,
470 42), as well as genes involved in sensation of chemical signals, such as those for TRP
471 channel homologs OCR-2 and OSM-9 (43, 44) and the cGMP-gated cation channel
472 TAX-4 (45), whose relationships to the 2-nonanone avoidance behavior have not been
473 studied.
474
475 *egl-3*, encoding a homolog of proprotein convertase, is required for neuropeptide
476 biosynthesis, expressed in many neurons, and known to be involved in various aspects
477 of worm behavior including learning (25, 41, 46). Deletion and missense mutations of
478 the gene are known to cause severe and mild phenotypes, respectively (25, 47). Our
479 previous study revealed that run duration is not increased after preexposure in *egl-3*
480 mutants, suggesting that neuropeptide signaling is required for the acquisition of odor
481 preexposure memory (25). In the present study, the abnormal features were similar
482 between deletion (*ok979*) and missense (*n589*) mutants, namely, run duration
483 (*Run_Dur*), odor concentration (*C_Ave*, *C_Ini*, *C_Ter*), and odor concentration change
484 (*dC_Ave*, *dC_Ter*), although the deletion mutants exhibited additional abnormal
485 features (Table 3 and Fig. 4). Increases in odor concentration in preexposed worms
486 were interesting because they were observed only in *egl-3* mutants but not in any other

487 mutants.

488

489 Mutations in *dop-3*, which encodes a homolog of the D2-type dopamine receptor, were
490 previously found to affect migratory direction after preexposure (25). This was
491 concluded because the mutants did not exhibit enhanced avoidance distance, although
492 run duration was increase after preexposure, and because run terminal bearing (*B_Ter*)
493 was worsened (25). These features were extracted in this analysis (Table 3), further
494 supporting the reliability of this analysis. In addition, the averaged directionality ratio
495 (*Dir_Ave*) was worsened (Table 3 and Fig. 4C). This is also consistent with the idea that
496 migratory direction is worsened in *dop-3* mutants after preexposure. Moreover, lowered
497 velocity (*V_Ave*, *V_Ter*; Table 3 and Fig. 4B) was also extracted, which may also
498 contribute to the failure in the enhanced odor avoidance. Such multiple abnormal
499 phenotypes are consistent with the fact that *dop-3* is expressed in many neurons and
500 involved in the regulation of multiple aspects of behavior (48).

501

502 *ocr-2* and *osm-9* both encode homologs of TRP-type cation channels, expressed in
503 multiple sensory neurons including ASH neurons and considered to be involved in
504 sensory perception as well as its modulation (43). We found that mutants for these two
505 genes did not exhibit significantly enhanced odor avoidance (Fig. 4A). In addition,
506 these mutants exhibited increases in velocity (*V_Ave* and *V_Ter*) after preexposure,
507 which was specific for these two mutants but not observed in other mutants. Some
508 features are specific for each mutant strains, which may reflect the differences in their
509 expression and/or function (43). Mutants of *tax-4*, encoding a homolog of the

510 cGMP-gated cation channel expressed in different sets of sensory neurons, exhibited a
511 unique pattern of features (Table 3, Fig. 4).
512
513 Taken together, our results suggest that the pattern of extracted features from mutant
514 strains may reflect functional groupings of the mutated genes. Thus, profiling and
515 classification of extracted mutant features of unknown genes may be useful to estimate
516 their physiological functions.
517
518 **Feature extraction of experience-dependent modulation of acoustic navigation of**
519 **bats**
520 To demonstrate the general applicability of our method, we examined features of
521 acoustic navigation in bats. We have previously reported that bats improve their flight
522 trajectory in an indoor space with obstacles in an experience-dependent manner
523 (Yamada et al., in revision). Here, we analyzed 42 features using gain ratios and
524 extracted several features, such as velocity (*V*), distance to the obstacle chain array
525 (*R_obs* and *R_x*), and horizontal bearing of the flight (*B_hori*) (Table 4 and Fig. 5A-C).
526 Interestingly, although velocity (*V*) itself was modulated by flight experience,
527 acceleration (*dV*) was not (Fig. 5D), suggesting that bats may determine flight speed
528 before initiating but not during navigation, at least in our experimental conditions.
529 Because the bats' vocalizations reflect their attention or decisions (49), our results
530 suggest that such higher brain functions during navigation could be extracted by
531 machine learning analysis.
532

533 **DISCUSSION**

534 In the present study, we extracted behavioral features that are modulated by experience
535 from olfactory navigation of worms and from acoustic navigation of bats using machine
536 learning analysis. In the case of worm olfactory navigation, we found a neural correlate
537 for one of the newly identified features: The reduced behavioral response to an increase
538 in odor concentration was consistent with the reduced response of ASH nociceptive
539 neurons to a small increase in odor concentration. In addition, we also found that mutant
540 strains can be grouped based on extracted features, which may correspond to the
541 physiological roles of genes in chemotaxis and/or experience-dependent modulation.
542 Furthermore, our machine learning analysis was applied to acoustic navigation of bats
543 to extract the features modulated by prior experience.

544

545 **Extraction of behavioral features by machine learning**

546 Machine learning has been playing a major role in classifying behavioral data of model
547 animals into several categories (7-13, 50). Instead of such behavioral classification,
548 however, we intended to use a machine learning technique for extracting characteristic
549 features of sensory behavior to decipher information processing in the brain. For that
550 purpose, we first hypothesized that a change in a behavioral feature reflects a change in
551 activity of a functional unit of the brain. Then, we used machine learning to extract
552 behavioral features that differ between two classes of behavior, rather than to categorize
553 the behavioral data into two classes; in our study, two classes (e.g., "with or without
554 prior experience" or "wild-type versus mutant strains") were determined *per se* and did
555 not need to be categorized.

556

557 In addition, we also included sensory information that worms experienced during the
558 course of behavior in the machine learning analysis. Although small model animals
559 such as *C. elegans* or *Drosophila melanogaster* are suitable for machine vision
560 monitoring and subsequent quantitative analysis of behavior, their small size makes it
561 difficult to measure sensory signals they receive during behavior. We have solved this
562 problem by precisely measuring the odor concentration at multiple spatio-temporal
563 points in a paradigm to asses olfactory behavior of worms (19), which allowed us to
564 include the information of odor concentration and its temporal changes (*C* and *dC*) into
565 the feature vector for the machine learning analysis. Our machine learning method
566 could also be used for detailed analysis of sensory navigation in the environment where
567 the gradients of chemical signal were also quantitatively monitored (36, 51, 52).

568

569 As a result, we were able to find multiple behavioral features modulated by prior
570 experience, including the temporal odor concentration change (*dC_Ter*), which was
571 consistent with the experience-dependent change in the responsiveness of ASH
572 nociceptive neurons. Such an effective and objective approach to estimate neural
573 function from comprehensive behavioral analysis may play important roles in the
574 understanding of recent large-scale monitoring of neuronal activity (see below).

575

576 For machine learning-based classification, support vector machines and deep learning
577 have also been used (53, 54). However, in these analyses, it is difficult for researchers
578 to understand which features are characteristic to each group because these algorithms

579 attempt to combine multiple features in a single representation. In other words, it is
580 difficult to use the results of classification for subsequent experiments and/or analysis to
581 further investigate the neural correlates of the behavioral differences. In contrast, in the
582 calculation of gain ratio, all features are evaluated independently, allowing us to
583 immediately translate the results of analysis to a new understanding and/or hypothesis
584 for subsequent experiments and analyses, as shown in the present study. Thus, we
585 conclude that the method used in this study—making a list of characteristic features
586 based on gain ratios and subsequently performing detailed analyses on each of extracted
587 features—is effective to understand the basic principles of neural functions regulating
588 behavior.
589
590 However, causal relationships among extracted features should be considered carefully.
591 For example, because odor concentration (*C*) and temporal odor concentration change
592 (*dC*) are both features of sensory stimuli, they were likely candidates for the cause of
593 changes in behavioral response. However, we regard that *dC*, rather than *C* itself, is the
594 causal reason because of the following: (1) previous quantitative analysis in the plate
595 assay paradigm revealed that pirouettes and runs are strongly correlated with positive or
596 negative *dC*, respectively, rather than the value of *C*; (2) in the OSB2 robotic
597 microscope system, positive or negative *dC* caused high or low levels of turning, such
598 as pirouettes and runs, respectively (19). For example, the lower *C* in preexposed
599 worms is likely caused by their relatively lower positions in the odor gradient (i.e.,
600 farther positions from the odor source) caused by the enhanced avoidance behavior. In
601 other words, sensory behaviors are closed loops—changes in sensory input cause

602 changes in behavior, while changes in behavior should also cause changes in sensory
603 input because the positions and/or directions of sensory organs are changed due to the
604 behavior. Thus, even when sensory features are extracted by machine learning, causal
605 relationships with behavioral features should be evaluated by independent experiments:
606 An open loop system, which allows control of sensory stimuli and monitoring behavior
607 independently, such as the OSB2 system (19), will provide an effective solution.
608
609 Analysis of multiple mutant strains revealed that the extracted features appeared to be
610 correlated with the physiological roles of the genes. For example, two alleles of a gene
611 required for neuropeptide signaling (*egl-3*) exhibited similar feature patterns, which
612 were different from mutants of a dopamine-signaling gene (*dop-3*). In addition,
613 mutations in two homologous but distinct TRP-type channel genes required for sensory
614 signaling (*ocr-2* and *osm-9*) exhibited a similar feature pattern, and the one for cyclic
615 nucleotide-gated ion channels (*tax-4*) exhibited a different pattern. It is interesting that
616 mutants of genes with similar functions exhibited similar behavioral features although
617 these genes should influence animal behavior in a complex manner. These results
618 suggest that behavioral features of mutants of a novel gene may be categorized to a
619 group of genes which have similar physiological functions. In other words, feature
620 extraction using gain ratio of multiple mutant strains can allow estimation of gene
621 functions in the nervous system.
622
623 In conclusion, we established a machine learning method to effectively reveal different
624 features of two different sensory behaviors. In particular, it is important to include not

625 only the behavior itself but also environmental sensory information that animals sense
626 in the feature vectors. Furthermore, it is also necessary to verify causal relationships of
627 the extracted features by other methods, such as using an open loop experimental setup.
628 In addition, this method can be used for estimation of the physiological function of
629 genes.
630
631 This method could be applied to analysis of more complex behaviors of other animals.
632 In the case of visual and acoustic stimuli, it is not clear what features of the stimuli (e.g.,
633 shapes, colors, and brightness for visual stimuli, and frequency and intensity for
634 acoustic stimuli) have the most prominent effects on behavior in a particular context.
635 We believe that our method presented herein, which allows extraction of the essential
636 features of information processing for sensory behaviors in the brain in an objective and
637 comprehensive manner, will help to solve this problem. Poor description of behavior
638 with simple indices compared to "big data" on neuronal activity is being recognized as
639 one of the significant problems in modern neuroscience (3-5). We expect that
640 comprehensive and objective feature extraction would increase the wealth of description
641 of behavior, which will provide us clues to understand more of the big data from brain
642 activity monitoring.
643
644 **FIGURE LEGENDS**
645 Figure 1. A workflow of the machine learning method for the analysis of worm odor
646 avoidance behavior; "Behavioral data" (Top) Examples of the trajectories of 3 worms
647 during 12 min of 2-nonanone avoidance assay, overlaid on a schematic drawing of a

648 9-cm agar plate. (Second from the top) A magnified view of trajectories of a worm, in
649 which runs are blue and pirouettes are red. (Second from the bottom and bottom)
650 Graphs showing the odor concentration (*C*, second from the bottom) and temporal
651 changes in *C* (*dC*, bottom) at the worm's position at 1-s intervals during the odor
652 avoidance assay. "Feature vector" From the (*x*, *y*) coordinates of each worm's centroid,
653 velocity, bearing, odor concentration, and their derivatives (*V*, *B*, *C*, *dV*, *dB*, and *dC*) as
654 well as the difference between the present and the previous values (Δ) were calculated.
655 "Gain ratio" One example (*C_Ter*) of calculating gain ratio is shown.
656
657 Figure 2. Extracted features that were modulated by prior experience of the odor. (A)
658 Enhanced odor avoidance behavior of worms caused by odor preexposure. (Left) End
659 points of 25 worms in each condition plotted on a schematic drawing of the assay plate.
660 (Right) Avoidance distance (distance between the center line of the plate and end point
661 of behavior) of each worm. Each bar represents median. Significant differences were
662 observed in the preexposed worms compared to the naive and mock-treated worms
663 (***$p < 0.001$, Kruskal-Wallis test with *post hoc* Dunn's test). (B, C, D and E)
664 Distributions of extracted features. Duration (B), the initial value of bearing change (C),
665 the average odor concentration (D), and the average odor concentration change (E) of
666 each run (**$p < 0.01$ and ***$p < 0.001$, Kruskal-Wallis test with *post hoc* Dunn's test).
667 t_{crit} for wild type worms was 13.1. Bars represent median and first and third quartiles.
668 (F) Time course changes in ensemble averages of odor concentration (*dC*) that worms
669 experienced before the termination of runs. On average, naive and mock-treated worms
670 experienced odor decrements of about -8 nM/s until 15 s before the end of each run,

671 when the decrements started to become very close to zero at the end of the run. In
672 contrast, preexposed animals consistently experienced smaller (i.e., shallower) odor
673 decrements during runs, and the average odor concentration changes at the end of runs
674 were positive. Bars represent mean ± SEM. (G) A model relationship between odor
675 concentration change and behavioral response during navigation along the odor gradient.
676 When naive and mock-treated worms sensed a slight increase in the odor concentration,
677 which is a sign of migrating in the wrong direction, they stopped a run and started a
678 pirouette to search for a new direction. In contrast, the preexposed worms did not
679 respond to a slight increase in odor concentration, leading to longer run durations and
680 shorter pirouette durations in total, which likely contribute to the enhanced avoidance
681 distance. Numbers of worms are 25 for all the conditions, and all the statistical details
682 are described in Supplementary Table 1.
683
684 Figure 3. Sensory responses to slight odor concentration increases were reduced by
685 preexposure to the odor. (A) A schematic drawing of calcium imaging of neural activity
686 of worms under odor stimuli. Several immobilized worms were simultaneously exposed
687 to an odor flow whose concentration was changed by controlling syringe pumps. (B)
688 Responses (GCaMP/mCherry) of ASH neurons in naive (n = 25), mock-treated (n = 29),
689 and preexposed (n = 26) worms. Thick colored lines with gray shadows indicate mean ±
690 SEM, and thin lines indicate individual responses. (C) Distributions of peak values
691 during the odor-increasing phase (t = 40-80 s) shown in panel B. Bars represent median.
692 (***$p < 0.001$, Kruskal-Wallis test with *post hoc* Dunn's test).
693

694 Figure 4. Examples of extracted features of mutant strains. Avoidance distance (A), the
695 average velocity (B), the average migratory direction (C), and the initial odor
696 concentration (D) per run are shown. t_{crit} for each strain was 8.1 (*egl-3(n589)*), 7.2
697 (*egl-3(ok979)*), 18.1 (*dop-3(tm1356)*), 11.2 (*ocr-2(ak47)*), 17.8 (*osm-9(ky10)*), and 6.7
698 (*tax-4(p678)*). Thick bars represent statistical differences between preexposed worms
699 versus naive *and* mock-treated worms, suggesting differences caused by the odor
700 preexposure; thin bars represent statistical differences between preexposed worms
701 versus naive *or* mock-treated worms, which were not caused by the preexposure. (**$p <$
702 0.01 and ***$p < 0.001$, Kruskal-Wallis test with *post hoc* Dunn's test)
703
704 Figure 5. Experience-dependent changes in bat acoustic navigation. (A) Measurement
705 system for 3D flight trajectory of a bat during obstacle avoidance flight in a chamber.
706 (B) Representative flight trajectories of a bat in horizontal plane during repeated flight
707 in the obstacle course. The top figure combines the initial three (red) and last three
708 (blue) flight trajectories. Each behavioral feature was collected in three segments:
709 earlier, middle, and later terms. Bottom figure shows an expanded view of the earlier
710 term in the first flight. Definition of the horizontal bearing of the flight (*B_hori*),
711 distance (*R_obs*), and bearing (*B_obs*) of the bat to the nearest edge point of the
712 obstacle chain array, longitudinal directional distance to the frontal chain array (*R_x*),
713 and lateral directional distance to the inside pitch of the chains array (*R_y*) are indicated.
714 Time windows for the analysis of each behavioral feature were 0.1, 0.2, or 0.3 s before
715 or when ($t = 0$) passing through the chain array. (C) A list of extracted features of bat
716 acoustic navigation modulated by flight experience. (D) Distributions of *V(-0.3)* and

717 *dV(-0.3)* are plotted. Bars represent median and first and third quartiles. (*$p < 0.05$,

718 Kruskal-Wallis test with *post hoc* Dunn's test).

719

720

721 **ACKNOWLEDGEMENTS**

722 We thank Drs. A. Yamazoe-Umemoto for early stage of this work, K. Matsushita, K.

723 Hironaka, T. Degawa, and the Kimura lab members for suggestions and comments on

724 this work. Nematode strains were provided by the Caenorhabditis Genetics Center

725 (funded by the NIH Office of Research Infrastructure Programs P40 OD010440) and by

726 National Bioresource Project funded by the Ministry of Education, Culture, Sports,

727 Science and Technology (MEXT), Japan. This work was supported by Interdisciplinary

728 graduate school program for systematic understanding of health and disease (for S.J.Y.),

729 by KAKENHI 25249020 and JP16H06536 (for K.H.), JP16H06542 (for S.H.),

730 JP16H06539 (for T.M.), JP16H06545 (for K.D.K.) from the MEXT, by PRESTO

731 JPMJPR14D8 (for S.H.) by JST, and by Osaka University Co-Creation Program (for

732 T.M. and K.D.K.).

733

734 **AUTHOR CONTRIBUTIONS**

735 S.J.Y, T.M. and K.D.K. designed the experiments, S.J.Y, Y.I., F.H., K.F., Y.T., Y.Y.,

736 K.H., S.H. and K.D.K. performed the experiments, S.J.Y. and T.M. analyzed the data,

737 and S.J.Y. and K.D.K. wrote the manuscript. All authors reviewed the manuscript.

REFERENCES

1. Alivisatos AP, et al. (2012) The Brain Activity Map Project and the Challenge of Functional Connectomics. *Neuron* 74(6):970–974.

2. Landhuis E (2017) Neuroscience: Big brain, big data. *Nature* 541(7638):559–561.

3. Krakauer JW, Ghazanfar AA, Gomez-Marin A, MacIver MA, Poeppel D (2017) Neuroscience Needs Behavior: Correcting a Reductionist Bias. *Neuron* 93(3):480–490.

4. Gomez-Marin A, Paton JJ, Kampff AR, Costa RM, Mainen ZF (2014) Big behavioral data: psychology, ethology and the foundations of neuroscience. *Nat Neurosci* 17(11):1455–1462.

5. Anderson DJ, Perona P (2014) Toward a Science of Computational Ethology. *Neuron* 84(1):18–31.

6. Bishop CM (2006) *Pattern Recognition and Machine Learning* (Springer Verlag).

7. Vogelstein JT, et al. (2014) Discovery of Brainwide Neural-Behavioral Maps via Multiscale Unsupervised Structure Learning. *Science* 344(6182):386–392.

8. Kabra, M., Robie, A. A., Rivera-Alba, M., Branson, S., & Branson, K. (2013). JAABA: Interactive machine learning for automatic annotation of animal behavior. *Nat Meth*, *10*(1), 64–67.

9. Branson K, Robie AA, Bender J, Perona P, Dickinson MH (2009) High-throughput ethomics in large groups of *Drosophila*. *Nat Meth* 6(6):451–457.

10. Dankert H, Wang L, Hoopfer ED, Anderson DJ, Perona P (2009) Automated monitoring and analysis of social behavior in *Drosophila*. *Nat Meth* 6(4):297–303.

11. Baek J-H, Cosman P, Feng Z, Silver J, Schafer WR (2002) Using machine vision to analyze and classify *Caenorhabditis elegans* behavioral phenotypes quantitatively. *J Neurosci Methods* 118(1):9–21.

12. Brown AEX, Yemini EI, Grundy LJ, Jucikas T, Schafer WR (2013) A dictionary of behavioral motifs reveals clusters of genes affecting *Caenorhabditis elegans* locomotion. *Proc Natl Acad Sci USA* 110(2):791–796.

13. Stephens GJ, Johnson-Kerner B, Bialek W, Ryu WS (2008) Dimensionality and Dynamics in the Behavior of *C. elegans*. *PLoS Comput Biol* 4(4):e1000028.

14. Lockery SR (2011) The computational worm: spatial orientation and its neuronal basis in *C. elegans*. *Curr Opin Neurobiol* 21(5):782–790.

15. Suzuki H, et al. (2008) Functional asymmetry in *Caenorhabditis elegans* taste neurons and its computational role in chemotaxis. *Nature* 454(7200):114–117.

16. Chronis N, Zimmer M, Bargmann CI (2007) Microfluidics for in vivo imaging of neuronal and behavioral activity in *Caenorhabditis elegans*. *Nat Meth* 4(9):727–731.

17. Clark DA, Gabel CV, Gabel H, Samuel ADT (2007) Temporal activity patterns in thermosensory neurons of freely moving *Caenorhabditis elegans* encode spatial thermal gradients. *J Neurosci* 27(23):6083–6090.

18. Kimura KD, Miyawaki A, Matsumoto K, Mori I (2004) The *C. elegans* Thermosensory Neuron AFD Responds to Warming. *Curr Biol* 14(14):1291–1295.

19. Tanimoto Y, et al. (2017) Calcium dynamics regulating the timing of decision-making in *C. elegans*. *eLife* 6:13819.

20. Larsch J, Ventimiglia D, Bargmann CI, Albrecht DR (2013) High-throughput imaging of neuronal activity in *Caenorhabditis elegans*. *Proc Natl Acad Sci USA* 110(45):E4266–73.

21. Yemini E, Jucikas T, Grundy LJ, Brown AEX, Schafer WR (2013) A database of *Caenorhabditis elegans* behavioral phenotypes. *Nat Meth* 10(9):877–879.

22. Quinlan JR (1986) Induction of Decision Trees. *Mach Learn* 1(1):81–106.

23. Brenner S (1974) The genetics of *Caenorhabditis elegans*. *Genetics* 77(1):71–94.

24. Kimura KD, Fujita K, Katsura I (2010) Enhancement of odor avoidance regulated by dopamine signaling in *Caenorhabditis elegans*. *J Neurosci* 30(48):16365–16375.

25. Yamazoe-Umemoto A, Fujita K, Iino Y, Iwasaki Y, Kimura KD (2015) Modulation of different behavioral components by neuropeptide and dopamine signalings in non-associative odor learning of *Caenorhabditis elegans*. *Neurosci Res* 99:22–33.

26. Pierce-Shimomura JT, Morse TM, Lockery SR (1999) The fundamental role of pirouettes in *Caenorhabditis elegans* chemotaxis. *J Neurosci* 19(21):9557–9569.

27. Yamada Y, Hiryu S, Watanabe Y (2016) Species-specific control of acoustic gaze by echolocating bats, Rhinolophus ferrumequinum nippon and Pipistrellus abramus, during flight. *J Comp Physiol A* 202(11):791–801.

28. Gorelik R, Gautreau A (2014) Quantitative and unbiased analysis of directional persistence in cell migration. *Nat Protoc* 9(8):1931–1943.

29. Iino Y, Yoshida K (2009) Parallel use of two behavioral mechanisms for chemotaxis in *Caenorhabditis elegans*. *J Neurosci* 29(17):5370–5380.

30. Quinlan JR (1992) *C4.5* (Morgan Kaufmann, San Mateo).

31. Frank E, Hall MA, Witten IH (2016) The WEKA Workbench (Online Appendix). *Data Mining* (Morgan Kaufmann). Forth Edition.

32. Tian L, et al. (2009) Imaging neural activity in worms, flies and mice with improved GCaMP calcium indicators. *Nat Meth* 6(12):875–881.

33. Shaner NC, et al. (2004) Improved monomeric red, orange and yellow fluorescent proteins derived from *Discosoma sp.* red fluorescent protein. *Nat Biotech* 22(12):1567–1572.

818 34. Lewis JA, Wu CH, Berg H, Levine JH (1980) The genetics of levamisole
819 resistance in the nematode *Caenorhabditis elegans*. *Genetics* 95(4):905–928.

820 35. Zheng Y (2015) Trajectory Data Mining. *ACM Trans Intell Syst Technol* 6(3):1–
821 41.

822 36. Louis M, Huber T, Benton R, Sakmar TP, Vosshall LB (2008) Bilateral olfactory
823 sensory input enhances chemotaxis behavior. *Nat Neurosci* 11(2):187–199.

824 37. Kato S, Xu Y, Cho CE, Abbott LF, Bargmann CI (2014) Temporal responses of
825 *C. elegans* chemosensory neurons are preserved in behavioral dynamics. *Neuron*
826 81(3):616–628.

827 38. Teghtsoonian R (1971) On the exponents in Stevens' law and the constant in
828 Ekman's law. *Psycho Rev* 78(1):71–80.

829 39. Kaplan JM (1996) Sensory signaling in *Caenorhabditis elegans*. *Curr Opin*
830 *Neurobiol* 6(4):494–499.

831 40. Bargmann CI (2006) Chemosensation in *C. elegans*. *WormBook*:1–29.

832 41. Kass J, Jacob TC, Kim P, Kaplan JM (2001) The EGL-3 proprotein convertase
833 regulates mechanosensory responses of *Caenorhabditis elegans*. *J Neurosci*
834 21(23):9265–9272.

835 42. Suo S, Ishiura S, Van Tol HHM (2004) Dopamine receptors in *C. elegans*. *Eur J*
836 *Pharmacol* 500(1-3):159–166.

837 43. Tobin D, et al. (2002) Combinatorial expression of TRPV channel proteins
838 defines their sensory functions and subcellular localization in *C. elegans* neurons.
839 *Neuron* 35(2):307–318.

840 44. Colbert HA, Smith TL, Bargmann CI (1997) OSM-9, a novel protein with
841 structural similarity to channels, is required for olfaction, mechanosensation, and
842 olfactory adaptation in *Caenorhabditis elegans*. *J Neurosci* 17(21):8259–8269.

45. Komatsu H, Mori I, Rhee JS, Akaike N, Ohshima Y (1996) Mutations in a cyclic nucleotide-gated channel lead to abnormal thermosensation and chemosensation in *C. elegans*. *Neuron* 17(4):707–718.

46. Li C, Kim K (2008) Neuropeptides. *WormBook*:1–36.

47. Husson SJ, Clynen E, Baggerman G, Janssen T, Schoofs L (2006) Defective processing of neuropeptide precursors in *Caenorhabditis elegans* lacking proprotein convertase 2 (KPC-2/EGL-3): mutant analysis by mass spectrometry. *J Neurochem* 98(6):1999–2012.

48. Chase DL, Koelle MR (2007) Biogenic amine neurotransmitters in *C. elegans*. *WormBook*:1–15.

49. Moss CF, Surlykke A (2010) Probing the natural scene by echolocation in bats. *Front Behav Neurosci* 4. doi:10.3389/fnbeh.2010.00033.

50. Hong W, et al. (2015) Automated measurement of mouse social behaviors using depth sensing, video tracking, and machine learning. *Proc Natl Acad Sci USA* 112(38):E5351–E5360.

51. Gershow M, et al. (2012) Controlling airborne cues to study small animal navigation. *Nat Meth* 9(3):290–296.

52. Albrecht DR, Bargmann CI (2011) High-content behavioral analysis of *Caenorhabditis elegans* in precise spatiotemporal chemical environments. *Nat Meth* 8(7):599–605.

53. Burges CJC (1998) A tutorial on support vector machines for pattern recognition. *Data Mining and Knowledge Discovery* 2(2):121–167.

54. LeCun Y, Bengio Y, Hinton G (2015) Deep learning. *Nature* 521(7553):436–444.

Table 1. A list of behavioral features used for worms' olfactory navigation

Parameters	Definition
RunNum	Number of a run
RunTime	Start time of a run
RunDur	Duration of a run
PirDur	Duration of the previous pirouette
V_Ave	Average velocity during a run
V_Ini	Velocity at run initiation
V_Ter	Velocity at run termination
dV_Ave	Average acceleration during a run
dV_Ini	Acceleration at run initiation
dV_Ter	Acceleration at run termination
B_Ave	Bearing of migratory vector throughout a run
B_Ini	Bearing at run initiation
B_Ter	Bearing at run termination
dB_Ave	Average temporal changes in bearing
dB_Ini	Temporal changes in bearing at run initiation
dB_Ter	Temporal changes in bearing at run termination
C_Ave	Average odor concentration during a run
C_Ini	Odor concentration at run initiation
C_Ter	Odor concentration at run termination
dC_Ave	Average temporal changes in odor concentration during a run
dC_Ini	Temporal changes in odor concentration at run initiation
dC_Ter	Temporal changes in odor concentration at run termination
Dir_Ave	Average directionality ratio
Dir_Ini	Directionality ratio at run initiation
Dir_Ter	Directionality ratio at run termination
WV	Curving rate of a run
RunDurΔ	Current *RunDur* minus the previous *RunDur*
PirDurΔ	Current *PirDur* minus the previous *PirDur*
WVΔ	Current *WV* minus the previous *WV*
X_AveΔAve	Current *Ave* minus the previous *Ave*
X_AveΔIni	Current *Ave* minus the previous *Ini*
X_AveΔTer	Current *Ave* minus the previous *Ter*
X_IniΔAve	Current *Ini* minus the previous *Ave*
X_IniΔIni	Current *Ini* minus the previous *Ini*
X_IniΔTer	Current *Ini* minus the previous *Ter*
X_TerΔAve	Current *Ter* minus the previous *Ave*
X_TerΔIni	Current *Ter* minus the previous *Ini*
X_TerΔTer	Current *Ter* minus the previous *Ter*
(*X* = *V, dV, B, dB, C, dC, Dir*)	

Table 2. Extracted features of worms' olfactory navigation modulated by prior odor experience

naive vs pre-exp		mock vs pre-exp	
V_Ave	0.1796	***C_Ter***	0.1337
Run_Dur	0.1558	***C_Ave***	0.0998
dB_Ini	0.1349	***C_Ini***	0.0932
C_IniΔAve	0.1230	***dC_Ave***	0.0854
C_IniΔIni	0.1230	*dC_Ini*	0.0810
dB_TerΔIni	0.1191	***dC_Ter***	0.0749
dB_AveΔIni	0.1013	*dC_IniΔTer*	0.0722
C_Ave	0.0983	*dC_TerΔIni*	0.0490
C_Ter	0.0942	*dV_AveΔIni*	0.0478
dB_IniΔTer	0.0924	*dV_Ini*	0.0478
C_Ini	0.0914	*dV_Ave*	0.0364
dB_IniΔAve	0.0839	***Run_Dur***	0.0352
V_AveΔAve	0.0815	***dB_Ini***	0.0342
dC_Ter	0.0810	***dB_TerΔIni***	0.0304
Run_DurΔ	0.0785	***dB_AveΔIni***	0.0298
dC_Ave	0.0547		
C_AveΔTer	0.0394		
Pir_Dur	0.0326		

Bold letters indicate features shared between the two comparisons.

876 **Table 3. Summary of extracted features of wild-type and mutant strains that are modulated by prior odor experience**

strain	*RunDur*	*V_Ave*	*V_Ini*	*V_Ter*	*B_Ter*	*dB_Ini*	*C_Ave*	*C_Ini*	*C_Ter*	*dC_Ave*	*dC_Ter*	*Dir_Ave*	*RunNum*
wild-type	up					down	down	down	down	up	up		
egl-3(n589)							up	up	up				
egl-3(ok979)		down	down	down		down	up	up	up				
dop-3(tm1356)	up	down		down	up					up	up	down	
ocr-2(ak47)		up		up	up								
osm-9(ky10)	up	up		up									
tax-4(p678)													up

877 Only features with statistical differences between preexposed worms versus naive *and* mock-treated worms are shown.

878

Table 4. A list of behavioral features used for bats' acoustic navigation

Parameters	Definition
V(t)	Fight velocity in 3D space
dV(t)	Flight acceleration in 3D space
B_hori(t)	Absolut bearing of the flight vector in a horizontal plane
dB_hori(t)	Temporal change in bearing of the flight vector in a horizontal plane
ddB_hori(t)	Temporal acceleration in bearing of the flight vector in a horizontal plane
B_vert(t)	Absolut bearing of the flight vector in a vertical plane
B_obs(t)	Absolute bearing to the edge point of the nearest chain array
R_obs(t)	Distance from the bat to the edge point of the nearest chain array
R_x(t)	Longitudinal directional distance to the frontal chain array
R_y(t)	Lateral directional distance to the inside pitch of the chain array
dH(t)	Temporal change in flight height

t = -0.3, -0.2, -0.1, or 0 s. *B_obs(t)* and *R_x(t)* were not calculated for t = 0.

Figure 1

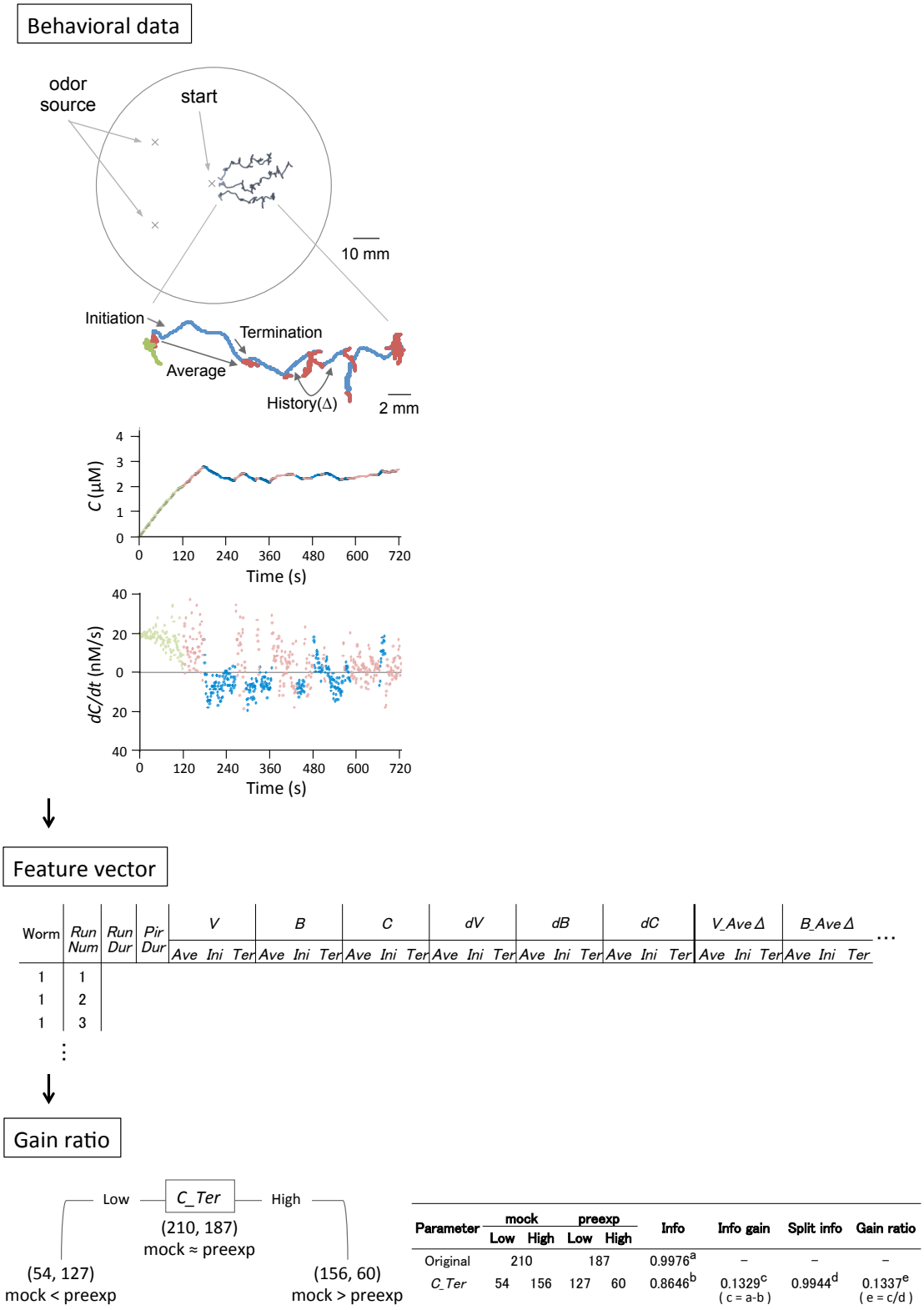

Parameter	mock Low	mock High	preexp Low	preexp High	Info	Info gain	Split info	Gain ratio
Original	210		187		0.9976[a]	–	–	–
C_Ter	54	156	127	60	0.8646[b]	0.1329[c] (c = a-b)	0.9944[d]	0.1337[e] (e = c/d)

Figure 2

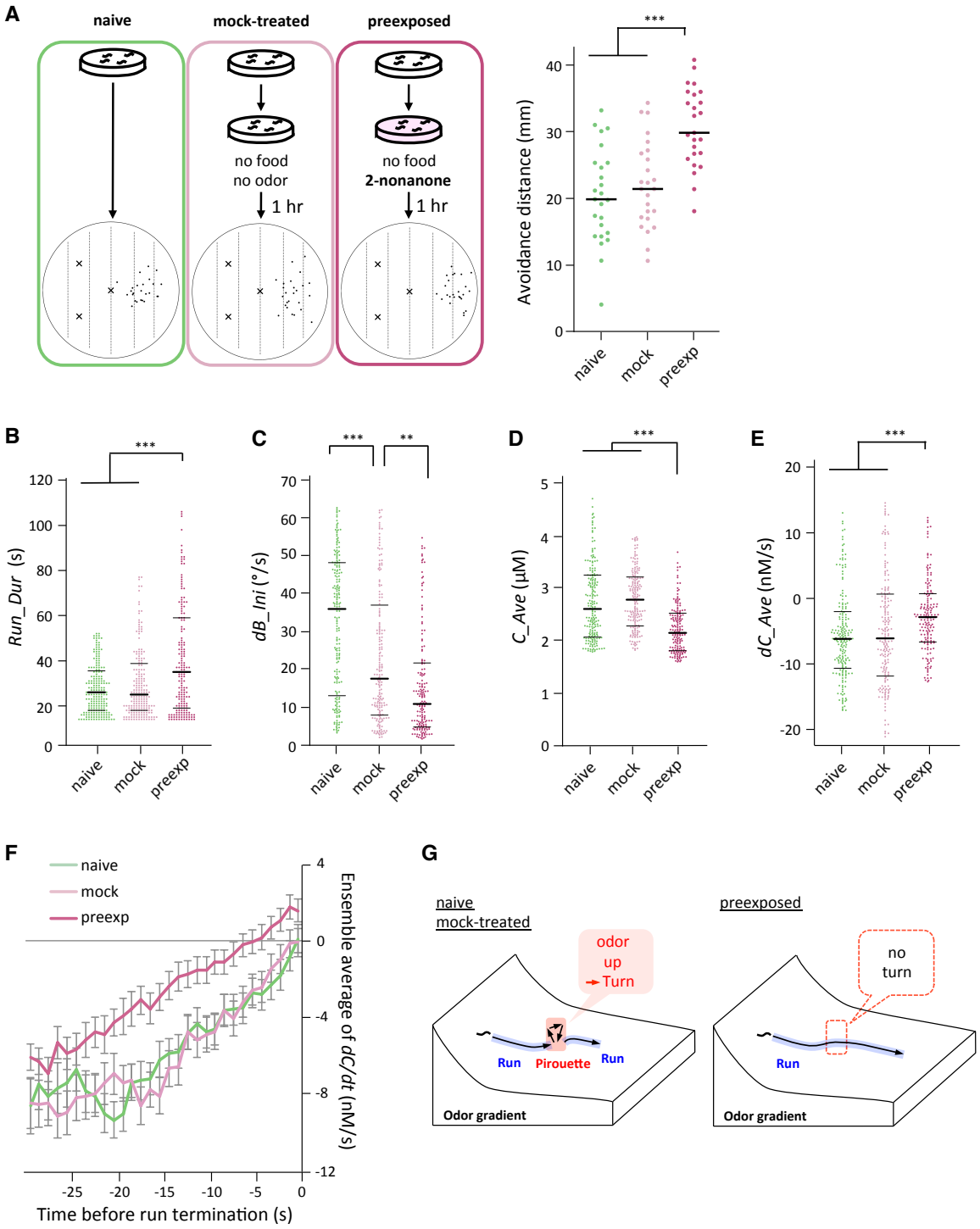
A
naive
mock-treated
preexposed
no food
no odor
1 hr
no food
2-nonanone
1 hr
Avoidance distance (mm)
***
naive
mock
preexp
B
Run_Dur (s)
***
C
dB_Ini (°/s)
***
**
D
C_Ave (µM)
***
E
dC_Ave (nM/s)
***
F
naive
mock
preexp
Ensemble average of dC/dt (nM/s)
Time before run termination (s)
G
naive
mock-treated
odor
up
Turn
Run
Pirouette
Run
Odor gradient
preexposed
no
turn
Run
Odor gradient

Figure 3

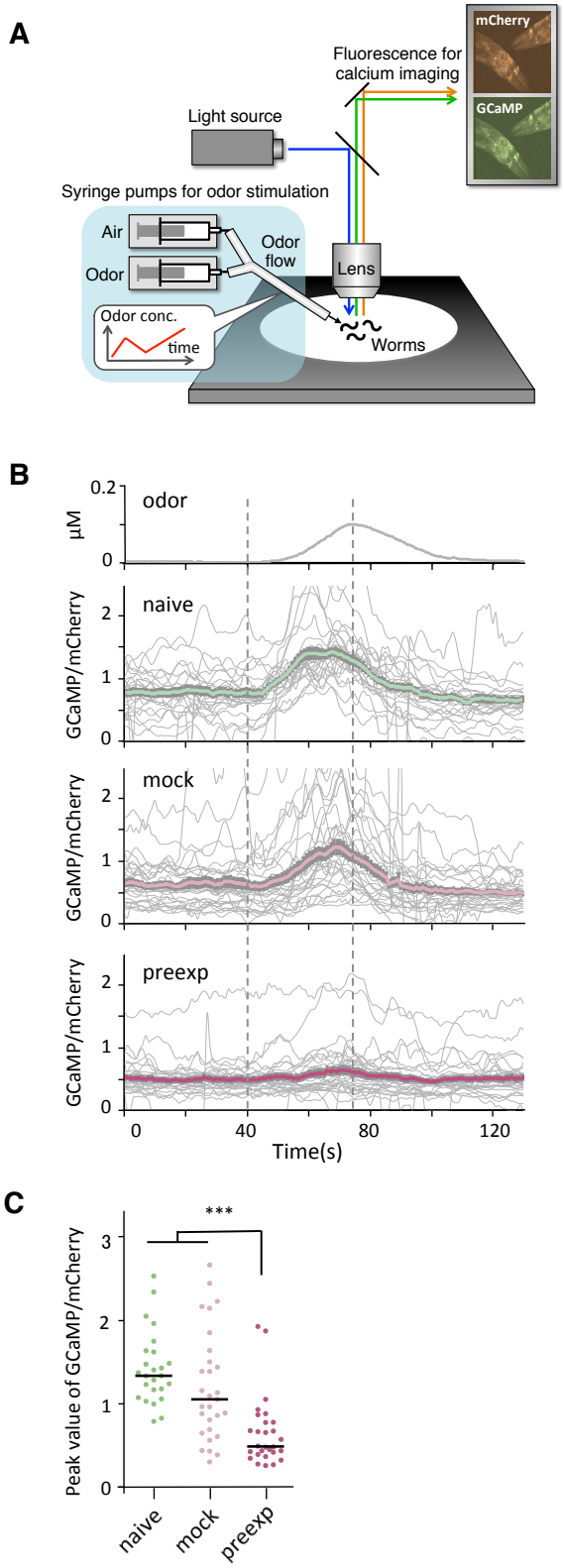
A
mCherry
GCaMP
Fluorescence for calcium imaging
Light source
Syringe pumps for odor stimulation
Air
Odor
Odor flow
Lens
Odor conc.
time
Worms
B
odor
μM
0.2
0
naive
mock
preexp
GCaMP/mCherry
2
1
0
0
40
80
120
Time(s)
C
***
Peak value of GCaMP/mCherry
3
2
1
0
naive
mock
preexp

Figure 4

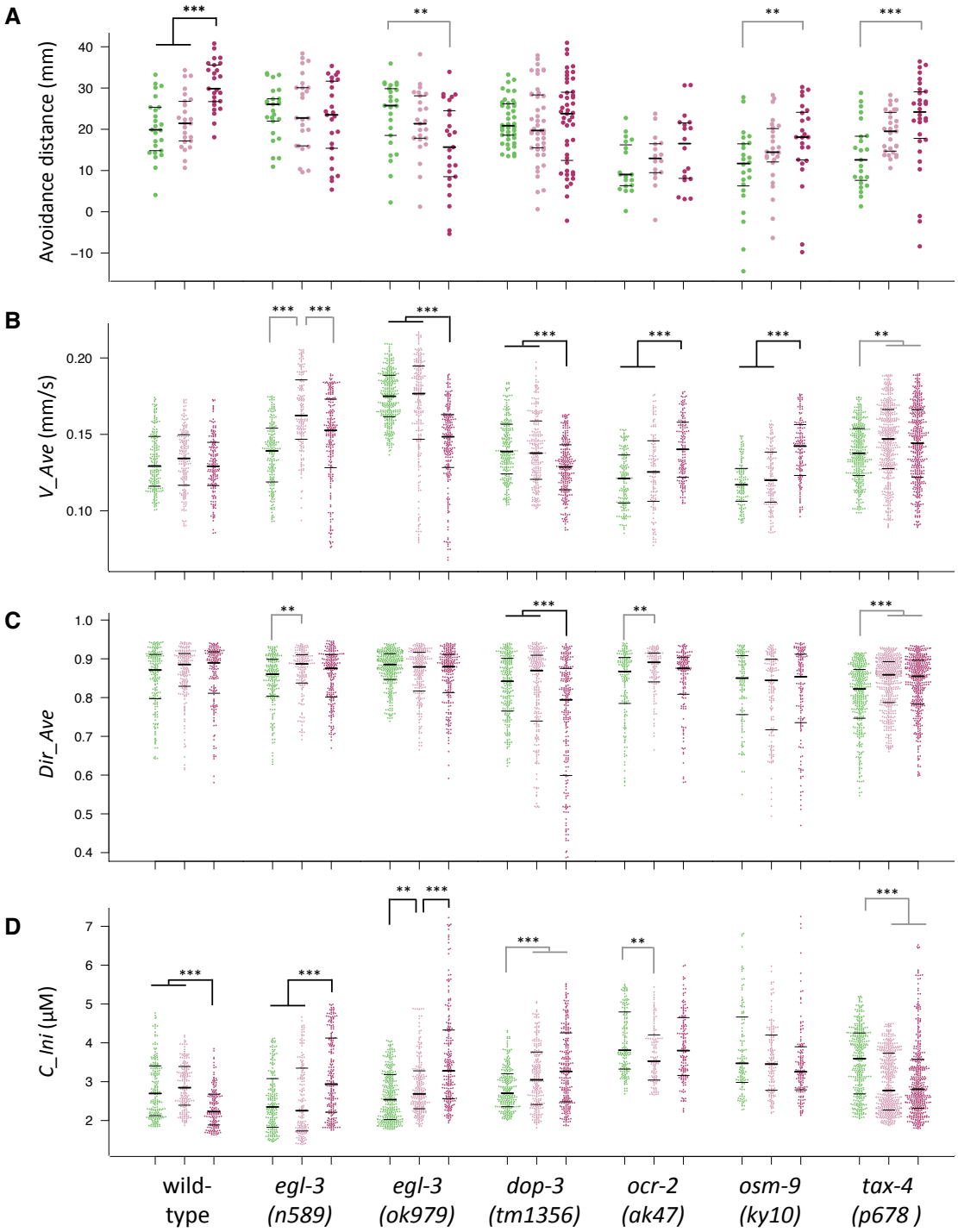
A
Avoidance distance (mm)
B
V_Ave (mm/s)
C
Dir_Ave
D
C_Ini (μM)
wild-type
egl-3 (n589)
egl-3 (ok979)
dop-3 (tm1356)
ocr-2 (ak47)
osm-9 (ky10)
tax-4 (p678)

Figure 5

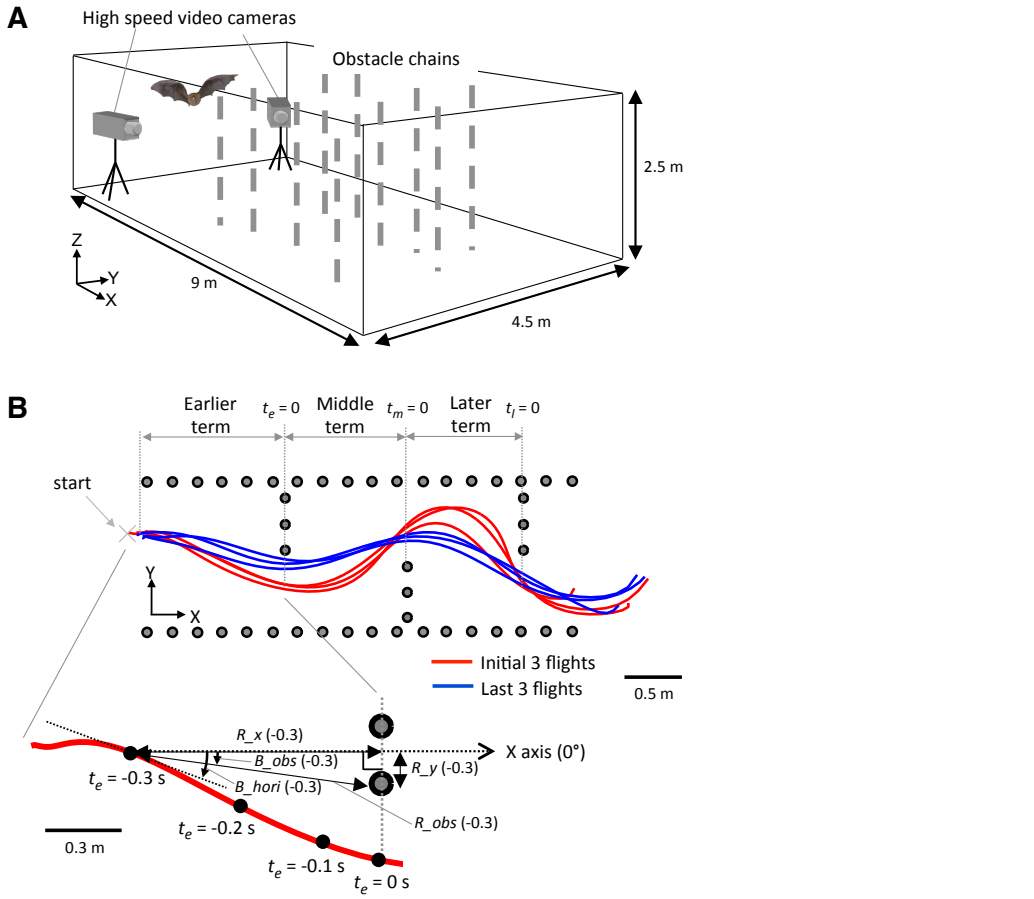

C

Features	Gain ratio
R_x (-0.3)	0.373
R_obs (-0.3)	0.352
V (-0.3)	0.312
V (-0.2)	0.294
R_x (-0.2)	0.294
R_obs (-0.2)	0.294
B_hori (-0.3)	0.292
B_hori (-0.2)	0.219
ddB_hori (-0.3)	0.209

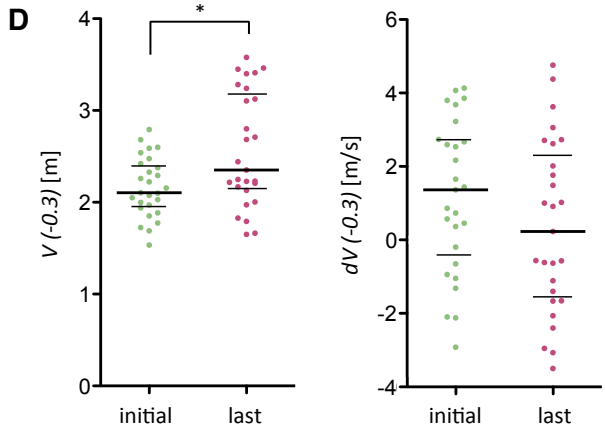

Supplementary Table 1

Supplementary Table 1. Detailed results of statistical tests.

Figure	Parameter	Number of naive	Number of mock	Number of preexp.	Unit of number	Multiple test	df value of multiple test	p value of multiple test	Other result of multiple test	Post-hock test	df value of post-hock test	p value of post-hock test	Other result of post-hock test
2A, 4A	Avoidance distance of N2	25	25	25	animals	Kruskal-Wallis test	2	<0.0001(***)	24.451	Dunn's test	1	naive vs mock: 0.7621(ns) naive vs preexposure: <0.0001(***) mock vs preexposure: 0.0001(***)	z = 0.6619 z = 4.5747 z = 3.9128
2B	Run duration of N2	219	210	187	runs	Kruskal-Wallis test	2	<0.0001(***)	18.76	Dunn's test	1	naive vs mock: 1(ns) naive vs preexposure: <0.0001(***) mock vs preexposure: 0.0006(***)	z = -0.4269 z = -3.9959 z = -3.547
2C	Initial dBearing of N2	219	210	187	runs	Mardia-Watson-Wheeler test	2	<0.0001(***)	64.69	Mardia-Watson-Wheeler test	1	naive vs mock: <0.0001(***) naive vs preexposure: <0.0001(***) mock vs preexposure: 0.002(**)	W = 26.305 W = 59.795 W = 12.007
2D	Average Conc. of N2	219	210	187	runs	Kruskal-Wallis test	2	<0.0001(***)	68.69	Dunn's test	1	naive vs mock: 0.1351(ns) naive vs preexposure: <0.0001(***) mock vs preexposure: <0.0001(***)	z = -1.6951 z = 6.3349 z = 7.9016
2E	Averege dConc. of N2	219	210	187	runs	Kruskal-Wallis test	2	0.0003(***)	16.56	Dunn's test	1	naive vs mock: 0.3202(ns) naive vs preexposure: <0.0001(***) mock vs preexposure: 0.0085(**)	z = -1.2441 z = -4.001 z = -2.7671
3C	Peak value of GCaMP3/mCherry	25	29	28	animals	Kruskal-Wallis test	2	<0.0001(***)	30.11	Dunn's test	1	naive vs mock: 0.0949(ns) naive vs preexposure: <0.0001(***) mock vs preexposure: 0.0004(***)	z = 1.8571 z = 5.3589 z = 3.6525
4A	Avoidance distance of *egl-3(n589)*	25	25	25	animals	Kruskal-Wallis test	2	0.7763(ns)	0.51	Dunn's test	1	-	-
4A	Avoidance distance of *egl-3(ok979)*	25	25	25	animals	Kruskal-Wallis test	2	0.0128(*)	8.72	Dunn's test	1	naive vs mock: 0.3924(ns) naive vs preexposure: 0.0051(**) mock vs preexposure: 0.1069(ns)	z = -1.1226 z = -2.9265 z = -1.8039
4A	Avoidance distance of *dop-3(tm1356)*	46	46	47	animals	Kruskal-Wallis test	2	0.8196(ns)	0.40	Dunn's test	1	-	-
4A	Avoidance distance of *ocr-2(ak47)*	19	16	18	animals	Kruskal-Wallis test	2	0.2001(ns)	3.22	Dunn's test	1	-	-
4A	Avoidance distance of *osm-9(ky10)*	24	26	24	animals	Kruskal-Wallis test	2	0.0191(*)	7.91	Dunn's test	1	naive vs mock: 0.1625(ns) naive vs preexposure: 0.0075(**) mock vs preexposure: 0.3141(ns)	z = 1.6058 z = 2.8055 z = 1.2552
4A	Avoidance distance of *tax-4(p678)*	23	29	30	animals	Kruskal-Wallis test	2	0.0008(***)	14.39	Dunn's test	1	naive vs mock: 0.0506(ns) naive vs preexposure: 0.0002(***) mock vs preexposure: 0.1175(ns)	z = 2.1232 z = 3.7932 z = 1.7605
4B	Average speed of N2	219	210	187	runs	Kruskal-Wallis test	2	0.2796(ns)	2.55	Dunn's test	1	-	-
4B	Average speed of *egl-3(n589)*	227	194	235	runs	Kruskal-Wallis test	2	<0.0001(***)	80.44	Dunn's test	1	naive vs mock: <0.0001(***) naive vs preexposure: <0.0001(***) mock vs preexposure: <0.0001(***)	z = -8.9653 z = -4.5544 z = 4.6671
4B	Average speed of *egl-3(ok979)*	370	260	252	runs	Kruskal-Wallis test	2	<0.0001(***)	137.51	Dunn's test	1	naive vs mock: 0.3296(ns) naive vs preexposure: <0.0001(***) mock vs preexposure: <0.0001(***)	z = 1.2272 z = 11.1444 z = 9.1734
4B	Average speed of *dop-3(tm1356)*	276	266	279	runs	Kruskal-Wallis test	2	<0.0001(***)	39.19	Dunn's test	1	naive vs mock: 0.6155(ns) naive vs preexposure: <0.0001(***) mock vs preexposure: <0.0001(***)	z = 0.8234 z = 5.795 z = 4.9154
4B	Average speed of *ocr-2(ak47)*	180	142	168	runs	Kruskal-Wallis test	2	<0.0001(***)	50.52	Dunn's test	1	naive vs mock: 0.075(ns) naive vs preexposure: <0.0001(***) mock vs preexposure: <0.0001(***)	z = -1.9599 z = -6.9657 z = -4.6254
4B	Average speed of *osm-9(ky10)*	147	175	160	runs	Kruskal-Wallis test	2	<0.0001(***)	66.85	Dunn's test	1	naive vs mock: 0.2053(ns) naive vs preexposure: <0.0001(***) mock vs preexposure: <0.0001(***)	z = -1.4875 z = -7.5979 z = -6.4146
4B	Average speed of *tax-4(p678)*	402	531	473	runs	Kruskal-Wallis test	2	<0.0001(***)	20.69	Dunn's test	1	naive vs mock: <0.0001(***) naive vs preexposure: 0.0019(**) mock vs preexposure: 0.3492(ns)	z = -4.456 z = -3.2307 z = 1.1931
4C	Average directionality ratio of N2	219	210	187	runs	Kruskal-Wallis test	2	0.2781(ns)	2.56	Dunn's test	1	-	-
4C	Average directionality ratio of *egl-3(n589)*	227	194	235	runs	Kruskal-Wallis test	2	0.0042(**)	10.96	Dunn's test	1	naive vs mock: 0.0014(**) naive vs preexposure: 0.1115(ns) mock vs preexposure: 0.1585(ns)	z = -3.3036 z = -1.7844 z = 1.6179
4C	Average directionality ratio of *egl-3(ok979)*	370	260	252	runs	Kruskal-Wallis test	2	0.1357(ns)	4.00	Dunn's test	1	-	-
4C	Average directionality ratio of *dop-3(tm1356)*	276	266	279	runs	Kruskal-Wallis test	2	<0.0001(***)	38.61	Dunn's test	1	naive vs mock: 1(ns) naive vs preexposure: <0.0001(***) mock vs preexposure: <0.0001(***)	z = -0.3986 z = 5.1836 z = 5.5349
4C	Average directionality ratio of *ocr-2(ak47)*	180	142	168	runs	Kruskal-Wallis test	2	0.0135(*)	8.62	Dunn's test	1	naive vs mock: 0.0062(**) naive vs preexposure: 0.6577(ns) mock vs preexposure: 0.0541(ns)	z = -2.8694 z = -0.7747 z = 2.0962
4C	Average directionality ratio of *osm-9(ky10)*	147	175	160	runs	Kruskal-Wallis test	2	0.6949(ns)	0.73	Dunn's test	1	-	-
4C	Average directionality ratio of *tax-4(p678)*	402	531	473	runs	Kruskal-Wallis test	2	<0.0001(***)	37.08	Dunn's test	1	naive vs mock: <0.0001(***) naive vs preexposure: <0.0001(***) mock vs preexposure: 1(ns)	z = -5.4554 z = -5.2773 z = 0.0423
4D	Initial Conc. of N2	219	210	187	runs	Kruskal-Wallis test	2	<0.0001(***)	57.75	Dunn's test	1	naive vs mock: 0.1381(ns) naive vs preexposure: <0.0001(***) mock vs preexposure: <0.0001(***)	z = -1.6846 z = 5.7215 z = 7.284
4D	Initial Conc. of *egl-3(n589)*	227	194	235	runs	Kruskal-Wallis test	2	<0.0001(***)	48.82	Dunn's test	1	naive vs mock: 1(ns) naive vs preexposure: <0.0001(***) mock vs preexposure: <0.0001(***)	z = 0.0374 z = -6.0955 z = -5.8855
4D	Initial Conc. of *egl-3(ok979)*	370	260	252	runs	Kruskal-Wallis test	2	<0.0001(***)	83.00	Dunn's test	1	naive vs mock: 0.002(**) naive vs preexposure: <0.0001(***) mock vs preexposure: <0.0001(***)	z = -3.2048 z = -9.0932 z = -5.4678
4D	Initial Conc. of *dop-3(tm1356)*	276	266	279	runs	Kruskal-Wallis test	2	<0.0001(***)	30.83	Dunn's test	1	naive vs mock: 0.001(***) naive vs preexposure: <0.0001(***) mock vs preexposure: 0.064(ns)	z = -3.4101 z = -5.4972 z = -2.0269
4D	Initial Conc. of *ocr-2(ak47)*	180	142	168	runs	Kruskal-Wallis test	2	0.0151(*)	8.38	Dunn's test	1	naive vs mock: 0.0057(**) naive vs preexposure: 0.2973(ns) mock vs preexposure: 0.1517(ns)	z = 2.8947 z = 1.2868 z = -1.6393
4D	Initial Conc. of *osm-9(ky10)*	147	175	160	runs	Kruskal-Wallis test	2	0.0637(ns)	5.51	Dunn's test	1	-	-
4D	Initial Conc. of *tax-4(p678)*	402	531	473	runs	Kruskal-Wallis test	2	<0.0001(***)	76.84	Dunn's test	1	naive vs mock: <0.0001(***) naive vs preexposure: <0.0001(***) mock vs preexposure: 0.8193(ns)	z = 8.0792 z = 7.3115 z = -0.6035

Figure	Parameter	Number of Groups	Number of initial	Number of last	Unit of number	Statistical tests used	p value	Other result
5D	Fight velocity in 3D space at t=−0.3	2	27	27	flights	Mann–Whitney test	0.0234(*)	Mann-Whitney U = 233.0
5D	Flight acceleration in 3D space at t=−0.3	2	27	27	flights	Mann–Whitney test	0.2326(ns)	Mann-Whitney U = 295.0